Final Report of Phase-II Research on

Applications of Active Adaptive Noise Control to Jet Engines

Prepared by:

Rahmat Shoureshi, Professor
Larry Brackney, PhD Candidate
Ray W. Herrick Labs
School of Mechanical Engineering
Purdue University
(317)-494-5639

Submitted to:

M. M. Bright
National Aeronautics and Space Administration
Lewis Research Center
Cleveland, OH

Grant No.: NAG3-1272

Grant Period: March 1, 1992 through February 28, 1993

EXECUTIVE SUMMARY:

During phase-II research on the application of active noise control to jet engines, the development of multiple-input/multiple-output (MIMO) active adaptive noise control algorithms and acoustic/controls models for turbofan engines were considered. Specific goals for this research phase included:

- Implementation of a MIMO adaptive minimum variance active noise controller
- Turbofan engine model development

A minimum variance control law for adaptive active noise control has been developed, simulated, and implemented for single-input/single-output (SISO) systems [1-4]. Since acoustic systems tend to be distributed, multiple sensors and actuators are more appropriate. As such, the SISO minimum variance controller was extended to the MIMO case. Simulation and experimental results are presented.

A state-space model of a simplified gas turbine engine is developed using the bond graph technique [5,6]. The model retains important system behavior, yet is of low enough order to be useful for controller design. Expansion of the model to include multiple stages and spools is also discussed.

MIMO MINIMUM VARIANCE CONTROLLER DEVELOPMENT:

Before discussing the adaptive MIMO minimum variance controller, it is important to recall some important results from [1-4]. First, an AutoRegressive Moving Average with eXogenous input (ARMAX) model structure is assumed for the system:

$$y(t) = \frac{B(z)}{A(z)} z^{-d} u(t) + \frac{C(z)}{A(z)} w(t)$$

where: A(z), B(z), and C(z) are polynomials in the unit delay operator, z; d is the time delay between the input, u(t), and the output, y(t); and w(t) is a white noise disturbance to the system.

The coefficients of the polynomials A(z) and B(z) may be identified using a Recursive Least Mean Squares (RLMS) algorithm. This simple iterative method consists of the following relations:

$$a_i(k+1) = a_i(k) + u_a \left(y(t) - \hat{y}(t)\right) y(t-d-i)$$

$$b_i(k+1) = b_i(k) + u_b \left(y(t) - \hat{y}(t)\right) u(t-d-i)$$

where: the a_i and b_i's are the estimated coefficients of the polynomials; u_a and u_b are the "learning" gains; and $\hat{y}$ is the estimated system output, given previous inputs, outputs and polynomial estimates.

Finally, a SISO minimum variance control law is given as:

$$u(t) = -\frac{\mu}{1+\mu}\hat{y}(t)$$

where: $\mu>0$.

The previous results are easily extended to the MIMO case. For multiple inputs and outputs, the ARMAX structure now becomes:

$$\overline{y}(t) = \begin{bmatrix} \frac{B_{11}}{A_1} z^{-d_{11}} & \cdots & \frac{B_{1n}}{A_1} z^{-d_{1n}} \\ \vdots & \ddots & \vdots \\ \frac{B_{n1}}{A_n} z^{-d_{n1}} & \cdots & \frac{B_{nn}}{A_n} z^{-d_{nn}} \end{bmatrix} \overline{u}(t) + \begin{bmatrix} \frac{C_1}{A_1} \\ \vdots \\ \frac{C_n}{A_n} \end{bmatrix} w(t)$$

In block diagram form, this relationship for a two-input/two-output system is shown as figure one.

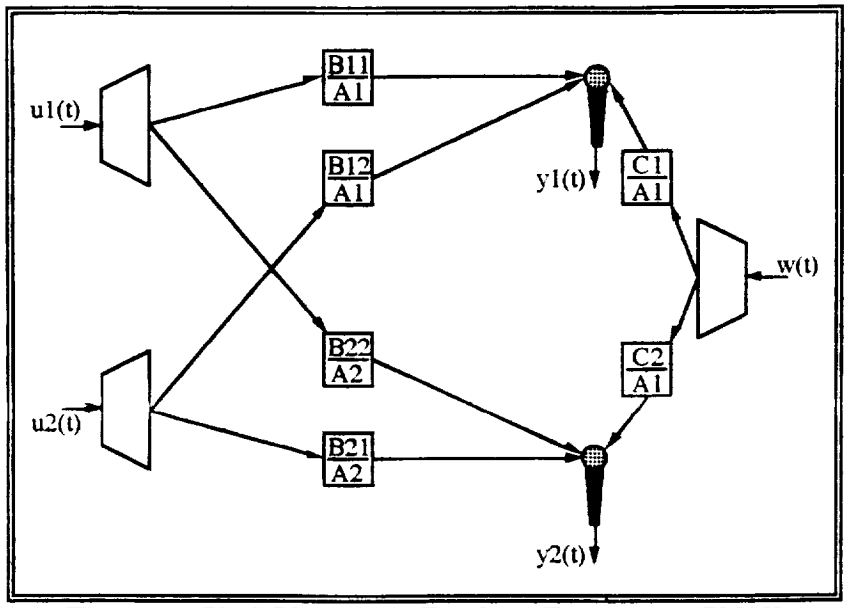

Figure one: Block Diagram of a Two-Input/Two-Output ARMAX Active Noise Control System

The multivariate RLMS algorithm is now expressed as a set of matrix iterations:

$$\begin{bmatrix} a_1(k+1) \\ \vdots \\ a_n(k+1) \end{bmatrix}_i = \begin{bmatrix} a_1(k) \\ \vdots \\ a_n(k) \end{bmatrix}_i + \begin{bmatrix} u_{a1} & 0 & 0 \\ 0 & \ddots & 0 \\ 0 & 0 & u_{an} \end{bmatrix} \begin{bmatrix} y_1(t) - \hat{y}_1(t) & 0 & 0 \\ 0 & \ddots & 0 \\ 0 & 0 & y_n(t) - \hat{y}_n(t) \end{bmatrix} \begin{bmatrix} y_1(t-d-i) \\ \vdots \\ y_n(t-d-i) \end{bmatrix}_i$$

$$\begin{bmatrix} b_{m1}(k+1) \\ \vdots \\ b_{mn}(k+1) \end{bmatrix}_i = \begin{bmatrix} b_{m1}(k) \\ \vdots \\ b_{mn}(k) \end{bmatrix}_i + \begin{bmatrix} u_{b1} & 0 & 0 \\ 0 & \ddots & 0 \\ 0 & 0 & u_{bn} \end{bmatrix} \begin{bmatrix} y_m(t) - \hat{y}_m(t) & 0 & 0 \\ 0 & \ddots & 0 \\ 0 & 0 & y_m(t) - \hat{y}_m(t) \end{bmatrix} \begin{bmatrix} u_1(t-d-i) \\ \vdots \\ u_n(t-d-i) \end{bmatrix}_i$$

Lastly, the MIMO minimum variance control law is:

$$\bar{u}(t) = -\begin{bmatrix} \frac{\mu_1}{1+\mu_1} & 0 & 0 \\ 0 & \ddots & 0 \\ 0 & 0 & \frac{\mu_n}{1+\mu_n} \end{bmatrix} \hat{y}(t)$$

A digital computer simulation has been developed to evaluate the MIMO adaptive minimum variance control structure. The simulated plant has the following ARMAX model:

$$\bar{y}(t) = \begin{bmatrix} \frac{z^2 - .2\,z + .02}{z^2 - 1.1\,z + .18} z^{-2} & \frac{.1\,z^2 - .02\,z + .002}{z^2 - 1.1\,z + .18} z^{-2} \\ \frac{.1\,z^2 - .00303\,z + .00101}{z^2 - .996\,z + .099} z^{-2} & \frac{z^2 - .0303\,z + .0101}{z^2 - .996\,z + .099} z^{-2} \end{bmatrix} \bar{u}(t) + \begin{bmatrix} \frac{z^2 - .8\,z + .32}{z^2 - 1.1\,z + .18} z^{-2} \\ \frac{.997\,z^2 - .981\,z + .454}{z^2 - .996\,z + .099} z^{-2} \end{bmatrix} w(t)$$

The initial model estimate is given as:

$$\hat{y}(t) = \begin{bmatrix} \frac{z^2 - .5\,z + .5}{z^2 - .5\,z + .5} z^{-2} & \frac{.1\,z^2 - .05\,z + .05}{z^2 - .5\,z + .5} z^{-2} \\ \frac{.1\,z^2 - .05\,z + .05}{z^2 - .5\,z + .5} z^{-2} & \frac{z^2 - .5\,z + .5}{z^2 - .5\,z + .5} z^{-2} \end{bmatrix} \bar{u}(t)$$

As a test of the RLMS algorithm, an initial simulation is run with $w(t)=0$, and $u_1(t)$ and $u_2(t)$ equal to the following input:

$$u_1(t) = u_2(t) = \begin{cases} .4\left[1.3 \sin(4.5\,\pi\,t) + .4 \sin(3 \cdot 4.5\,\pi\,t) + .25 \sin(5 \cdot 4.5\,\pi\,t)\right] & t < 2.25 \\ .02\left[1.3 \sin(10\,\pi\,t) + .4 \sin(3 \cdot 10\,\pi\,t) + .25 \sin(5 \cdot 10\,\pi\,t)\right] & 2.25 < t < 3.75 \\ .32\left[1.3 \sin(1.9\,\pi\,t) + .4 \sin(3 \cdot 1.9\,\pi\,t) + .25 \sin(5 \cdot 1.9\,\pi\,t)\right] & t > 3.75 \end{cases}$$

This input is the Fourier series approximation of a square wave. Enough terms are retained such that the signal is sufficiently exciting. The frequency and amplitude of the square wave are also varied in order to test the robustness of the adaptation algorithm.

Figures two and three compare the two system outputs with their corresponding estimates. The estimates appear to converge within one-half of a second. Changes in the signal have no apparent effect on the output estimate.

Closed-loop simulations are obtained by using the MIMO minimum variance control law, and setting w(t) equal to the square wave given previously. Figures four and five compare the open-loop response (controller off), the closed-loop response, and the estimate of the closed-loop output. Clearly, the controller is effective in attenuating the time-varying noise disturbance. The closed-loop estimate does not converge on the actual system output because the exogenous input term, C(z)/A(z) w(t), is unmodeled by the controller. Since w(t) is unmeasurable, the coefficients of C(z) may not be determined using an algorithm such as RLMS.

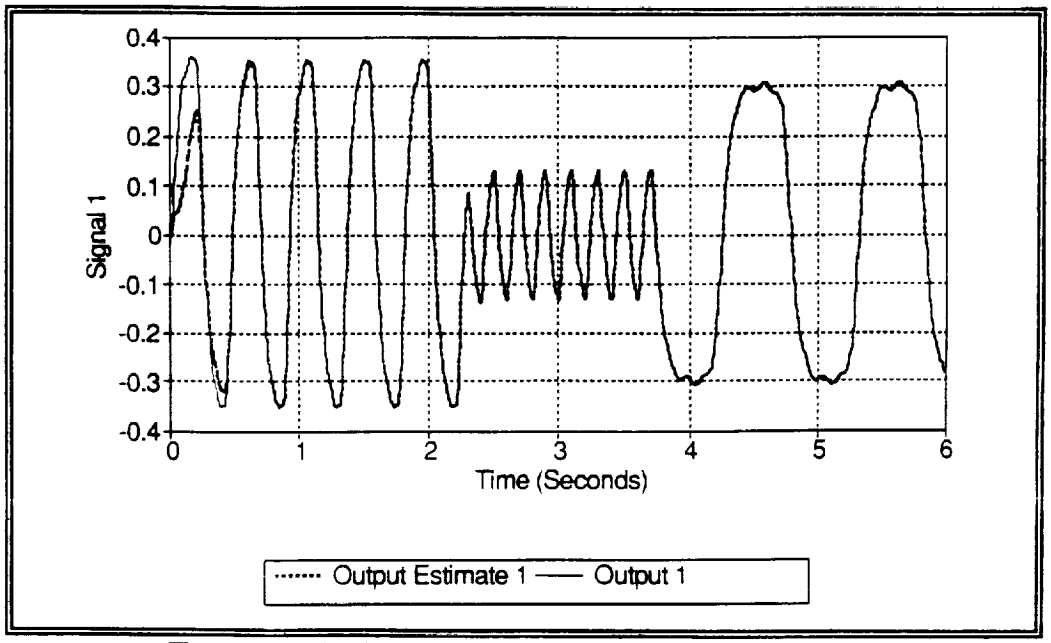

Figure two: Simulated Open-Loop Test of the RLMS Algorithm:
A Comparison of Output One and Its Estimate

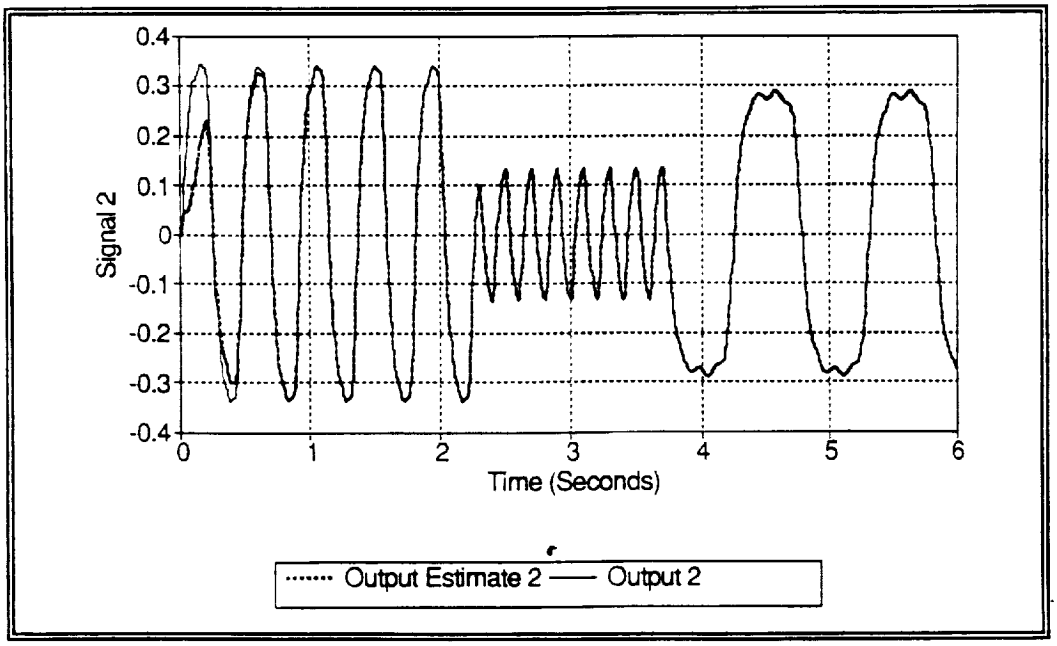

Figure three: Simulated Open-Loop Test of the RLMS Algorithm:
A Comparison of Output Two and Its Estimate

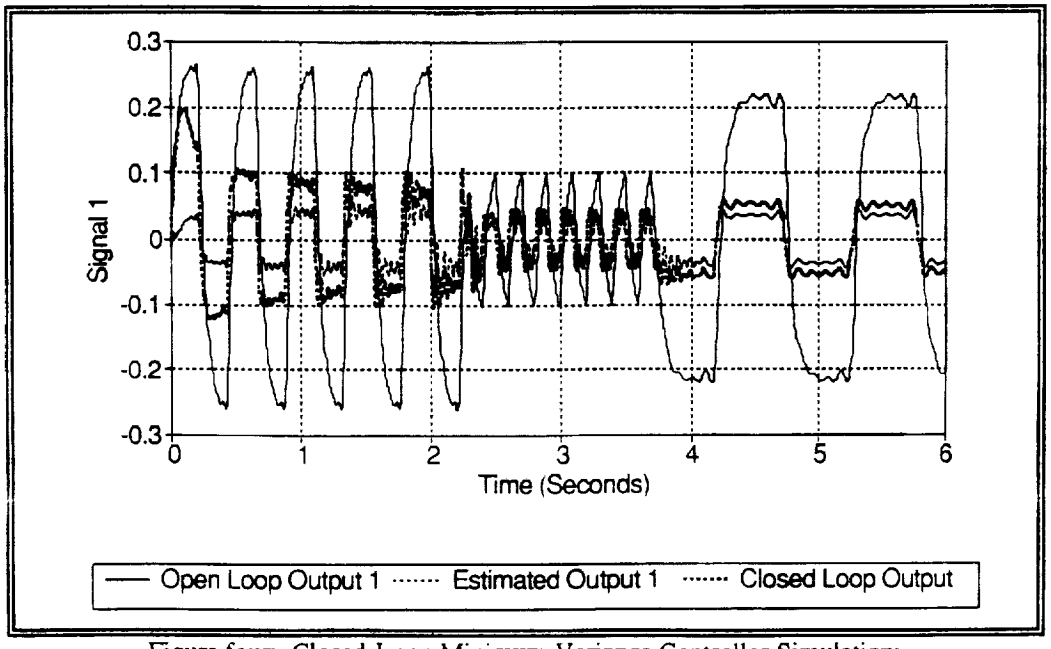

Figure four: Closed-Loop Minimum Variance Controller Simulation:
A Comparison of Controlled and Uncontrolled Output One and Its Estimate

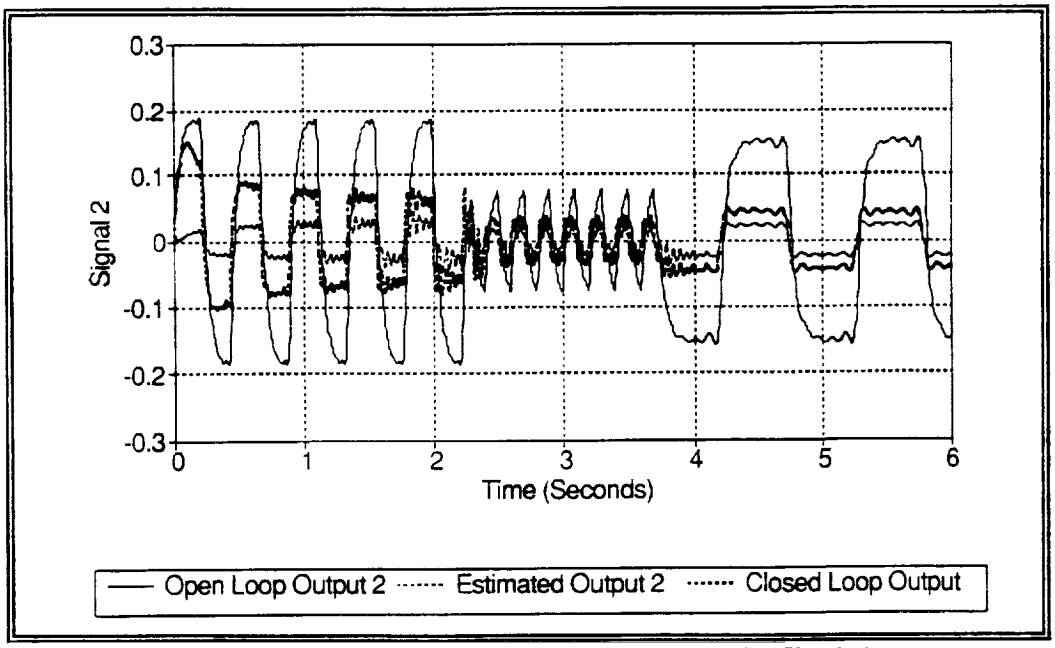

Figure five: Closed-Loop Minimum Variance Controller Simulation:
A Comparison of Controlled and Uncontrolled Output Two and Its Estimate

A MIMO adaptive minimum variance active noise controller has been implemented as a Turbo Pascal program on a 25 MHz 386-based PC. A Metrabyte DAS-20 data acquisition and control card provides the interface to the two microphones and speakers used in the experiment. A third speaker acts as a noise source, and is driven by a sinusoidal input. Noise cancellation experiments are conducted in a typical laboratory environment with the same speaker/microphone geometry shown in figure one.

Figures six, seven, and eight illustrate the convergence of the B_{11}, A_1, and A_2 polynomials from the RLMS algorithm, as well as the resulting error between the output and its estimate. It is important to note that the initial values for the coefficients have a very important role in the numerical stability and convergence of the estimation algorithm. This is not the case for the SISO controller. The MIMO RLMS performance is much less robust than its SISO counterpart, in that 22 coefficients must converge properly as opposed to the previous seven coefficients. This lack of robustness degrades both stability and performance. The change in controller effectiveness is obvious from the insertion loss plots given in figure nine.

The MIMO controller exhibited the ability to adapt to changes in speaker/microphone geometry and acoustic impedance. Small changes in speaker and microphone placement did not affect performance significantly. Additionally, foam blocks were inserted in the acoustic path with no apparent change in the level of sound attenuation.

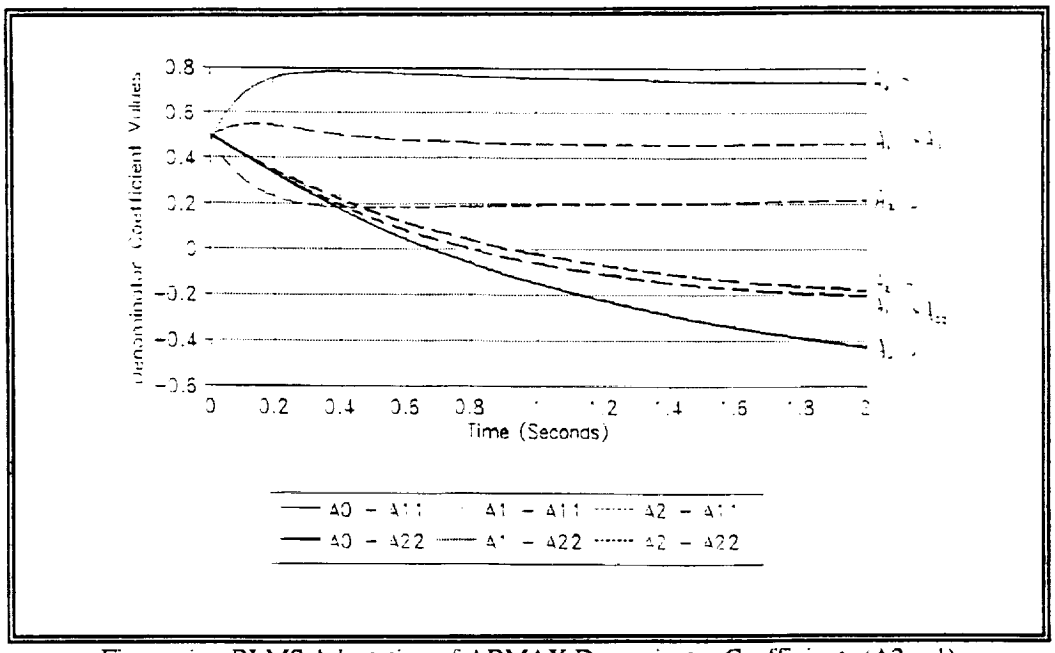

Figure six: RLMS Adaptation of ARMAX Denominator Coefficients (A3 = 1)

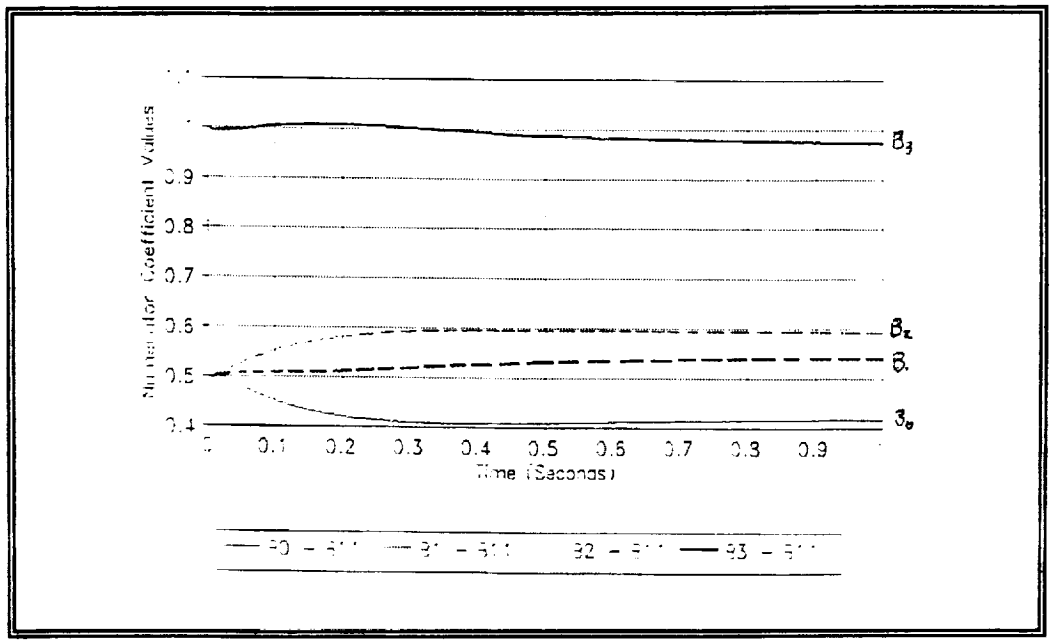

Figure seven: RLMS Adaptation of ARMAX Numerator Coefficients for Polynomial B11

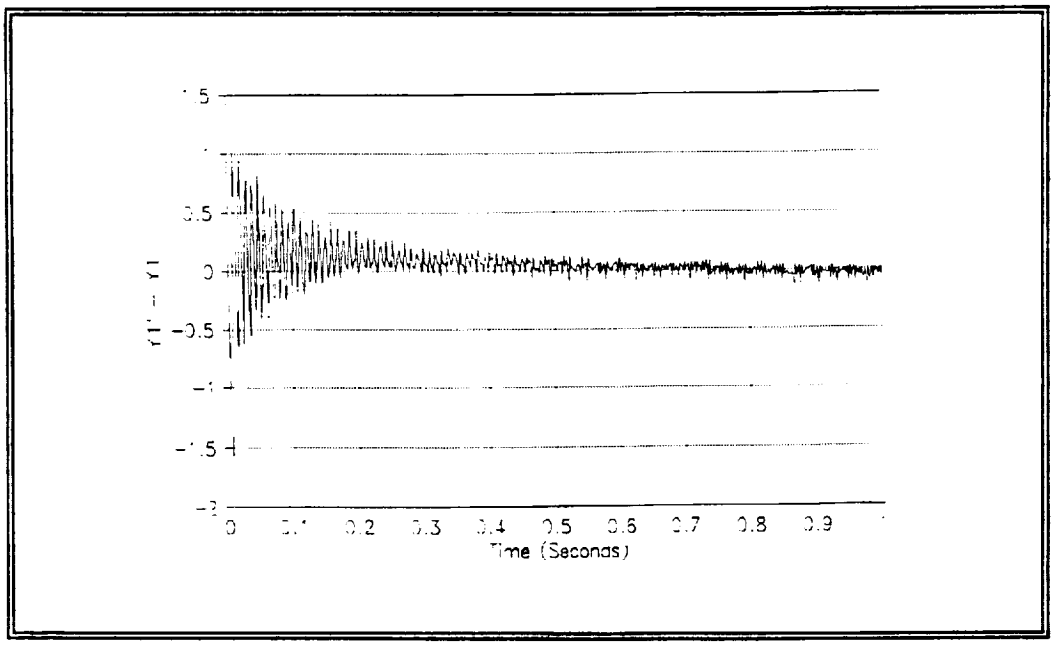

Figure eight: Error Between Measured Plant Output and Estimated Output from ARMAX Model

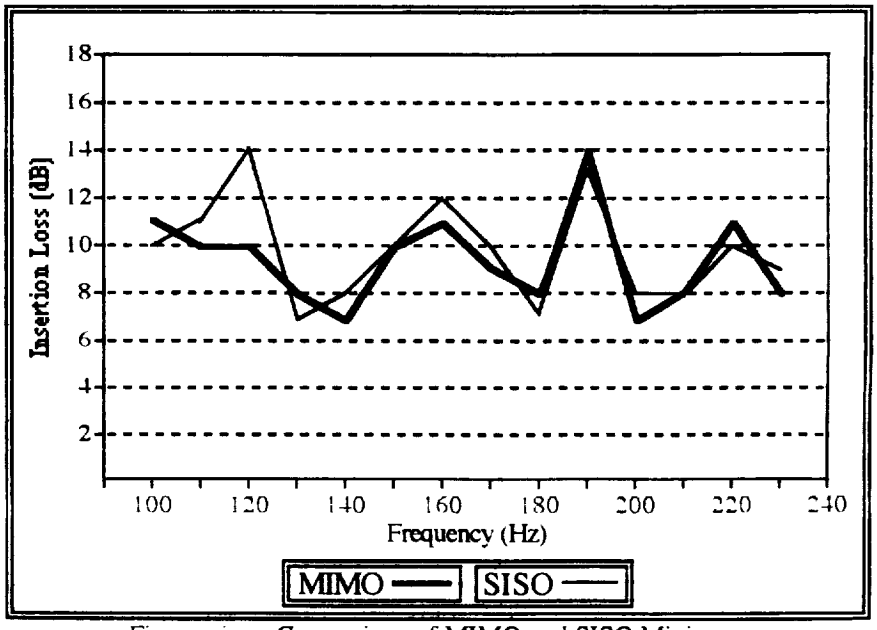

Figure nine: Comparison of MIMO and SISO Minimum Variance Controller Performance

ENGINE MODEL DEVELOPMENT:

A great deal of effort is spent by the research community in the area of gas turbine modelling. Typically, such models are highly complex, and represent the dynamics of only one engine component, e.g. an axial flow compressor model [7]. Researchers attempt to describe system behavior with systems of partial differential equations, or more recently, differential equations which lead to chaos.

While such models are useful for engine design and analysis, they are not appropriate for control design purposes. This need has motivated the development of state space models for control synthesis. One such model, HYTESS, is a four state model of a hypothetical twin-spool turbofan engine [8]. Proprietary state space models for specific engines also exist. Unfortunately, the simplicity of these models comes at a price - a lack of information concerning the internal pressure dynamics of the engine. The inclusion of internal pressures in the system state is crucial if the model is to be used for noise control. Clearly, a new state space model is needed.

The bond graph technique pioneered by Paynter seems well suited for modelling turbomachinery, as it provides a uniform methodology for modelling mechanical, thermal, and fluid energy modes. Compressors and turbines are special cases of a general turbomachine in which interactions between the thermal and fluid domains result in shaft power (turbine), or compression of the fluid (compressor). Figure ten depicts this energy exchange as a simple bond graph [5].

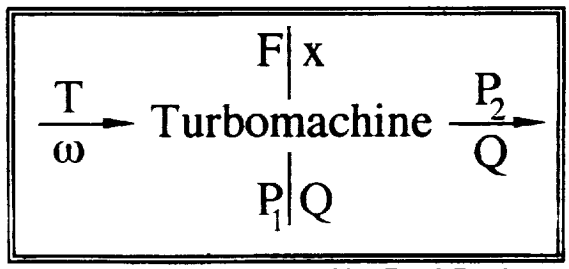

Figure ten: A Simple Turbomachine Bond Graph

A typical gas turbine is composed of several components: a compressor, a combustor, a turbine, a shaft to transfer work from the turbine to the compressor, and an exit nozzle. In practice, turbofan engines are comprised of multiple compressor and turbine stages along with more than one driving shaft. The model developed here is for the simpler single stage case which appears as figure eleven. Extension to a more realistic engine representation is not difficult, as will be shown shortly.

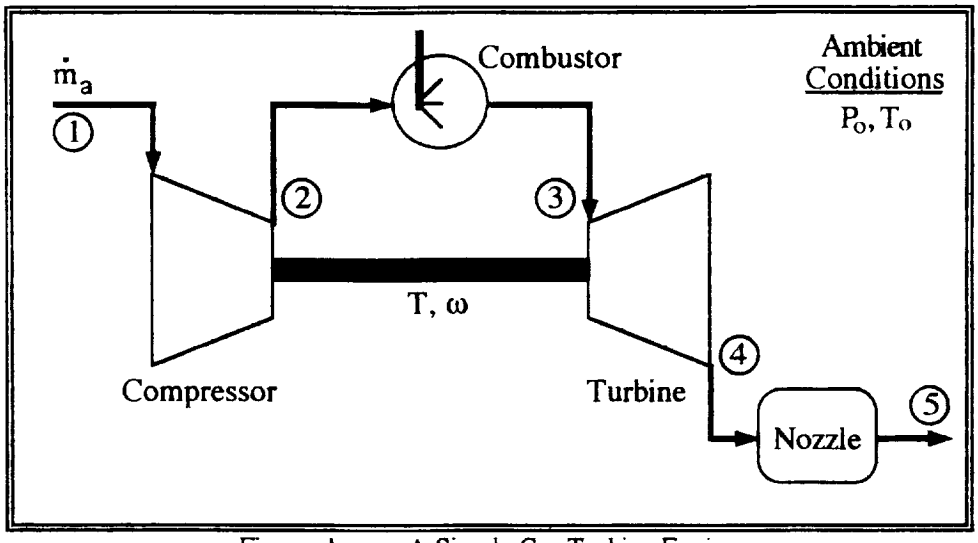

Figure eleven: A Simple Gas Turbine Engine

The energy flow, or power, associated with each component in a gas turbine engine is effected by one or more of the following mechanisms:

- Resistance (Nozzles) - R
- Capacitance (Fluid compressibility) - C
- Inertance (Fluid flow) - I

Each component of the gas turbine engine may be described by a "basic functional unit" (BFU) bond graph comprised of these "R", "C", and "I" elements [6]. Since temperature and heat flow are used as energy variables, the resulting model is a pseudo bond graph. The model describes the relationships between pressure, mass flow, torque, and engine speeds as well as temperature and heat flow, and is shown in figure twelve.

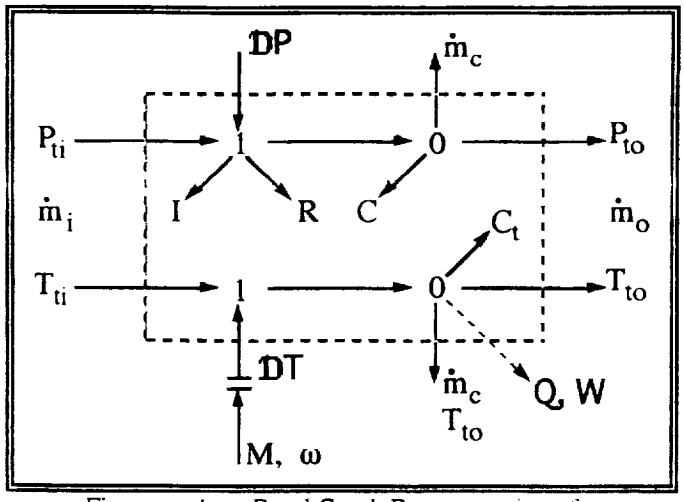

Figure twelve: Bond Graph Representation of a "Basic Functional Unit"

The fundamental differential equations governing the generic BFU are found by applying constitutive laws between effort and flow variables. They are:

$$\frac{d}{dt}\dot{m}_i = \frac{1}{I}\left[P_{ti} + \mathbf{D}P_t - R\,\dot{m}_i\right]$$

$$\frac{d}{dt}P_{to} = \frac{1}{C}\left[\dot{m}_i - \dot{m}_c - \dot{m}_o\right]$$

$$\frac{d}{dt}T_{to} = \frac{C_p}{C_T}\left[\dot{m}_i\left(T_{ti} + \mathbf{D}T_t\right) - \dot{m}_o\,T_{to} - \dot{m}_c\,T_{to} + (\dot{Q}\text{ or }\dot{W})\right]$$

The complete bond graph for the simplified gas turbine appears in figure thirteen, and is obtained by cascading multiple BFUs and eliminating unnecessary elements.

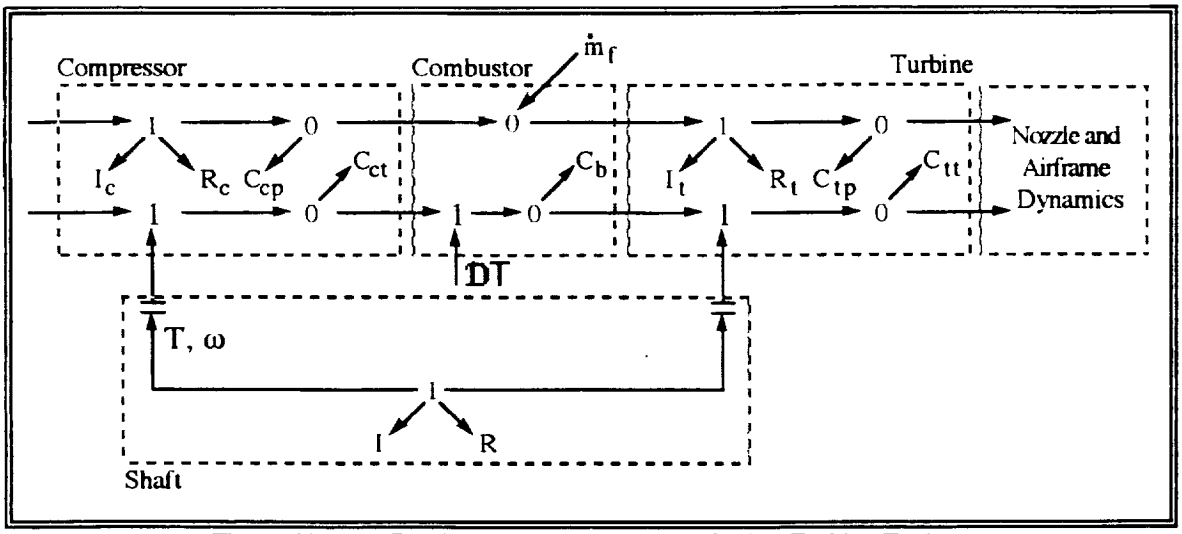

Figure thirteen: Bond Graph Representation of a Gas Turbine Engine

The differential equations describing the complete bond graph are:

$$\frac{d}{dt}\dot{m}_{ci} = \frac{1}{I_c}\left[P_o - R_c\,\dot{m}_{ci}\right]$$

$$\frac{d}{dt}P_{co} = \frac{1}{C_{cp}}\left[\dot{m}_{ci} - (\dot{m}_{ti} - \dot{m}_f)\right]$$

$$\frac{d}{dt}T_{co} = \frac{C_p}{C_{ct}}\left[\dot{m}_{ci}\,T_o - (\dot{m}_{ti} - \dot{m}_f)\,T_{co} + \eta_c\,\mathbf{T}\,\omega\right]$$

$$\frac{d}{dt}T_{bo} = \frac{C_p}{C_b}\left[(\dot{m}_{ti} - \dot{m}_f)\,T_{co} - \dot{m}_{ti}\,T_{bo} + \eta_b\,\Delta H_c\,\dot{m}_f\right]$$

$$\frac{d}{dt}\dot{m}_{ti} = \frac{1}{I_t}\left[P_{co} - R_t\,\dot{m}_{ti}\right]$$

$$\frac{d}{dt}P_{to} = \frac{1}{C_{tp}}\left[\dot{m}_{ti} - \dot{m}_{to}\right]$$

$$\frac{d}{dt} T_{to} = \frac{C_p}{C_{tt}} \left[\dot{m}_{ti} T_{bo} - \dot{m}_{to} T_{to} - \eta_t \mathbf{T} \omega \right]$$

$$\frac{d}{dt} \omega = \frac{1}{I_s} \left[\mathbf{T} - R_s \omega \right]$$

At first glance these eight state equations appear to be linear, however, the "R", "I", and "C" parameters are functions of the state as well as physical parameters associated with the gas turbine [6]. The parametric relationships are given as:

$$I \equiv \frac{L}{A} = \frac{\text{Component Length}}{\text{Effective Component Cross-Sectional Area}}$$

$$C_p \equiv \frac{LA}{n R T} = \frac{\text{Component Volume}}{\text{(Polytropic Index) (Gas Constant) (Outlet Temperature)}}$$

$$C_t \equiv \frac{n c_p L A P}{R (n-1) \gamma T} = \frac{\text{(Constant Terms) (Volume) (Outlet Pressure)}}{\text{(Constant Terms) (Outlet Temperature)}}$$

Although the polytropic index, n, is lumped with other "constant terms," it is important to note that it may also be a variable depending on the nature of the process. Namely, whether it is assumed isothermal or isentropic, n would change from a minimum to a maximum value.

A linearized model of the system is obtained by selecting reasonable values for the physical parameters, selecting an operating point, and taking a Taylor series expansion about that point. The parameters used in the model are given in Table one.

Parameter	Value	Parameter	Value
L_c	1 m	η_c	0.8
A_c	2.64 m^2	η_t	0.9
L_t	1 m	η_b	0.98
A_t	2.64 m^2	ΔH_c	4.3×10^7 $J/_{kg}$
L_b	0.5 m	C_p	1005 $J/_{kg\,K}$
γ	1.4	n	1.35
R_c	1.2 $N\,s/_{kg\,m^2}$	R_t	0.7 $N\,s/_{kg\,m^2}$
R_s	1.7 $kg\,m2/_s$	R	287.1 $J/_{kg\,K}$

Table one: Gas Turbine Parameters Used for Linear Model Development

Figure fourteen represents the responses of both the compressor and turbine outlet pressures to a step change in fuel flow. The pressure ratio of this engine appears to be 6:1. Perhaps of greater interest, are the frequency response plots of the two pressures with respect to the fuel flow input shown as figure fifteen. A lightly damped pair of poles affect the response at 334 rad/sec in our single stage model. High noise levels in this frequency range have been reported in previous experimental studies. Simply adding additional BFU's to the bond graph (representing additional turbine and/or compressor stages for example) could produce more peaks.

The parameters used in the preparation of this model may not be representative values of actual engine parameters. The bond graph techniques shown here provide a convenient means of generating structured models of desired order, however, some means of parameter identification is needed to complete the model. Results from more sophisticated simulations or (preferably) actual engine frequency spectra could be used to complete this task.

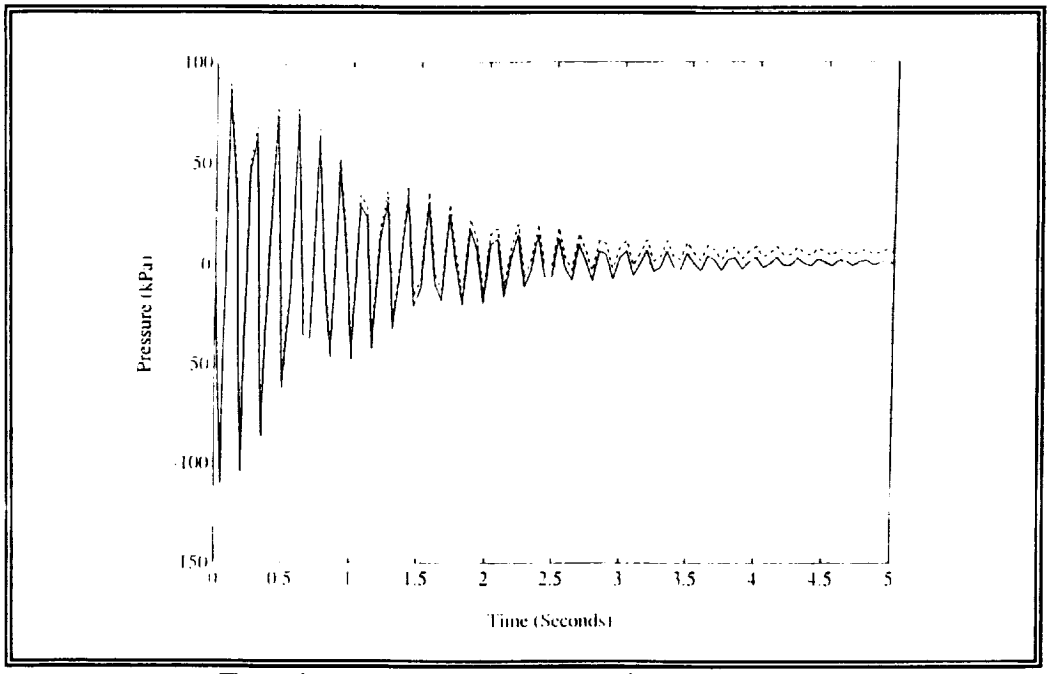

Figure fourteen: Pressure Responses for the Compressor and Turbine Outlets for a Step Change in Fuel Flow

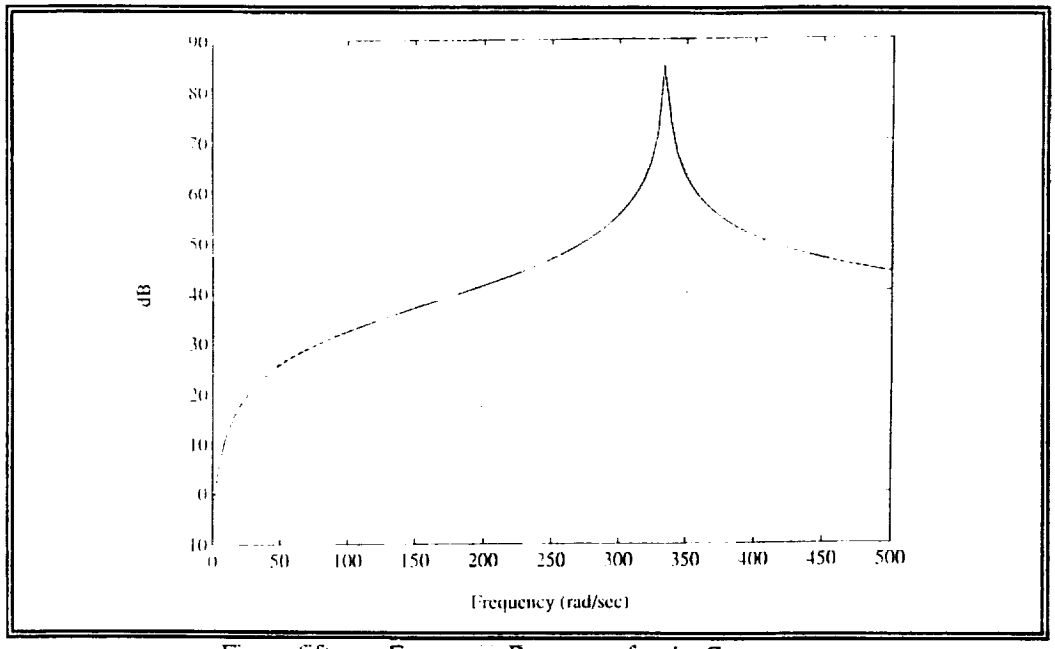

Figure fifteen: Frequency Responses for the Compressor and Turbine Outlet Pressures effected by the Fuel Flow

CONCLUSIONS:

A Multiple-Input/Multiple-Output adaptive minimum variance controller has been developed for active noise cancellation. The controller has been shown to be effective in simulation. The controller implementation was also successful at attenuating pure tone disturbances, and was able to adapt to changes in speaker/microphone geometry as well as acoustic impedance. The MIMO controller performance did not represent a significant improvement over the SISO controller in the experimental setup used during the implementation stage. MIMO controller performance appears to be limited by the lack of robustness of the RLMS algorithm used to identify system parameters.

A framework for developing state space models of gas turbine engines suitable for acoustic controller design has been discussed. Bond graph model components are cascaded to represent multi-stage compressor and turbine systems. This modular approach allows a great deal of flexibility in determining appropriate model order and shaping the open loop characteristics. Some form of parameter identification is required before such a model would be of use. A hypothetical gas turbine model is presented in order to illustrate the types of results which could be obtained from a more sophisticated multi-stage model with properly identified parameters.

SUGGESTIONS FOR FUTURE RESEARCH:

The RLMS algorithm used for on-line parameter identification in the MIMO minimum variance controller exhibits a lack of robustness. This can lead to stability problems and poor attenuation. An alternate method of parameter identification using neural networks has been proposed by Chu and Shoureshi [9, 10]. Such techniques may improve both the stability and performance of an adaptive controller.

The adaptive minimum variance control structure has been the focus of this study. An adaptive pole placement controller was also evaluated, but was abandoned due to the computational complexity it required. It is unclear if the conservative designs of robust control methodologies such as H_∞ and QFT are appropriate for noise control. Nevertheless, it would be of interest to evaluate these and other advanced control structures with regards to the noise cancellation problem.

A multi-stage turbofan engine model is required for noise controller design and evaluation. The modelling approach presented here is meant to serve as a starting point for such research. Parameter identification and experimental verification of the model are important parts of this process.

Finally, an important issue which must be addressed is the selection of actuation and sensing mechanisms for this application. Control inputs must be identified which satisfy the controllability requirements of the nonlinear, time-varying system of a jet engine. Similarly, the dual problem of sensor selection and observability must be considered. The harsh conditions which these sensors and actuators would be subjected to make this a challenging problem.

ACKNOWLEDGEMENTS:

The researchers are grateful to the Rose-Hulman Institute of Technology for the use of some of their facilities during an experimental portion of this study. We are also appreciative of the support and encouragement provided by Michelle Bright, Carl Lorenzo, Walter Merrill, and others in the NASA Lewis research center Advanced Controls Technology group.

REFERENCES:

1. Shoureshi, R., Brackney, L., Kubota, N., and Batta, G., "A modern control approach to active noise control," ASME Publication #G90550, 1990.

2. Shoureshi, R. and Matsuyoshi, Y., "Design and implementation of self-tuning regulators for active noise control," Proceedings of the ASME Computers in Design Conference, 1991.

3. Brackney, L., Shoureshi, R., Bright, M., and Lorenzo, C., "A comparison of adaptive control techniques applied to active noise cancellation," Proceedings of the ASME Winter Annual Meeting, 1992.

4. Shoureshi, R. and Brackney, L., "Final report of phase-I research on applications of active adaptive noise control to jet engines", Presented to NASA-Lewis, November, 1991.

5. Paynter, H. M., "The dynamics and control of Eulerian turbomachines," ASME Journal of Dynamic Systems and Control, 1972.

6. Krikelis N. and Papadakis, F., "Gas turbine modelling using pseudo-bond graphs", International Journal of Systems Science, 1988.

7. Lawless, P. and Fleeter, S., "Active unsteady aerodynamic suppression of rotating stall in an incompressible flow centrifugal compressor with vaned diffusor," AIAA-91-1898, Presented at the AIAA 27th Joint Propulsion Conference, 1991.

8. Merrill, W., Beattie, E., et al., "HYTESS- A Hypothetical Turbofan Engine Simplified Simulation," NASA-TM-83561, 1984.

9. Chu., R. and Shoureshi, R., "Identification of Dynamical Systems Using Neural Networks," Proceedings of the 13th IMACS World Congress, Dublin, Ireland, Vol. 3, pp. 1375-1376, July 1991.

10. Chu, R. and Shoureshi, R., "Neural-Based Adaptive Nonlinear System Identification," DSC-Vol. 45, Intelligent Control Systems, ASME-WAM, pp. 55-62, November 1992.